MDPI

Article

Lithofacies Characteristics and Controlling Factors of Fine-Grained Sedimentary Rocks in the Lower First Member of the Shahejie Formation in the Northern Lixian Slope of Raoyang Sag, China

Yuezhe Li , Jie Yin * and Zhenqi Wang

School of Geosciences, Yangtze University, Wuhan 430100, China
* Correspondence: yinjiecr7@yangtzeu.edu.cn

Abstract: In order to further explore the potential of unconventional oil and gas in the northern Lixian Slope of Raoyang Sag, the lithofacies types and their controlling factors of the lower first member of the Shahejie Formation (Es_1L) in the Xiliu area were analyzed through the comprehensive application of core log studies, micro-sections and their magnified analyses, mineral suits recognitions with XRD, and major and organic geochemistry. The results show that the lacustrine sedimentary rocks of Es_1L in the Xiliu area comprise five lithofacies types: medium organic silty mixed fine-grained rock, medium organic massive clay rock, high organic shale calcareous mixed fine-grained rock, high organic matter shale calcareous clay rock, and high organic matter shale limestone. The vertical variation of the characteristic element reflects that the deposition in Es_1L has different stages; that is, the bottom of Es_1L is formed with low source influence, high water salinity, and strong reduction conditions, while the upper fine-grained rocks are formed in a sedimentary environment with high source influence, low water salinity, and weak reduction conditions. The change of the sedimentary environment controls the development of lithofacies and the occurrence of organic matter. These results advocate for the basic research of fine-grained sedimentary rocks in the faulted lacustrine basin aid for further unconventional oil and gas exploration.

Keywords: Raoyang Sag; paleoenvironment; Shahejie Formation; fine-grained sedimentary rock; lithofacies

1. Introduction

High-resolution imaging reveals that fine-grained sediments contain clay and silt-size fractions with particle sizes of less than 0.0625 mm [1,2]. Their components are predominantly felsic minerals (quartz, potassium feldspar, plagioclase, etc.), clay minerals (illite, chlorite, montmorillonite, etc.), carbonate minerals (dolomite, calcite, etc.), and other authigenic minerals. Mudstone and shale are the main lithologies of fine-grained sediments [3–5]. Their formation has undergone a complex sedimentary process, and the shale laminae are developed, with a thickness of 10–500 μm that changes frequently in a lesser thickness range. Different types of laminae, such as siliceous laminae, carbonate laminae, and organic laminae, have different geochemical characteristics and formation mechanisms [6,7]. The investigations of lithofacies and small-scale sedimentary characteristics of mudstone are guides for the evaluation of reservoir-forming factors in unconventional oil and gas exploration [8–10]. The current practices in the lithofacies analysis methods for fine-grained sedimentary rocks are direct observation, numerical reconstruction, and a geochemical analysis method [11–15].

Raoyang Sag in Bohai Bay Basin is rich in oil and gas resources [16–19]. It is challenging to increase oil and gas production in Raoyang Sag, and there is a call for alternative resources. The lower first member of the Shahejie Formation (Es_1L) in the Sag belongs to the special lithologic section (limestone mudstone, limestone, mudstone, and shale

interbedding) in the lacustrine transgression period. The identification of the lithofacies types of the special lithologic section has a theoretical guiding role for subsequent unconventional oil and gas exploration in the study area [20]. Specifically based on core analysis, micro-petrography, whole rock X-ray diffraction, and geochemistry, we identified the lithofacies of fine-grained sedimentary rocks in Es_1L in the Xiliu area in the northern Lixian slope, and discussed the relationship between lithofacies variation, organic matter, and water environment changes in lake sediments.

2. Geological Setting

The Lixian slope in the west of Raoyang Sag in the Bohai Bay Basin is a large-scale wide and gentle sedimentary slope developed on the Middle and Upper Proterozoic carbonate rocks [21,22]. It is NE trending, connected to Baoding Sag in the west, Suning, Dawangzhuang structural belt, and Renqiu buried hill belt in the East; Baxian Sag in the north, Liucun-Shenze low uplift, and Jinxian Sag in the south [23–25]. It is 20–30 km wide from east to west, and about 80 km long from north to south. The exploration area is about 2000 km^2, accounting for about one third of the area of Raoyang Sag (Figure 1). The selected study area is located in Xiliu area, connected with Renxi Sag to the north of the Lixian slope. There is a set of fine-grained sediments deposited in the maximum lake transgression in Es_1L in the middle and northern part of Raoyang Sag, composed of oolitic limestone, oil shale, dolomitic limestone, black mudstone, and shales. The average depth of a single well is about 3320–3390 m, with stable development and a thickness of 30–200 m. It is among one of the good source rock sections in Raoyang Sag.

The Raoyang Sag is filled with thick Paleogene sediments comprising the Kongdian Formation, Shahejie Formation, and Dongying Formation [26]. Among them, the Shahejie Formation can be divided into four members named Es_4, Es_3, Es_2, and Es_1, whereas Es_1 can be further divided into lower and upper parts (Figure 2). The lower submember of Es_1 is developed in the fault extension stage, and the upper submember of Es_1 is developed in the fault uplift and extinction stage [27]. Fine-grained sediments dominated by tractive flow are developed in the first member of the Lixian slope. The sandstone at the bottom of the lower first member is developed in the shallow delta front subfacies environment when the lake level is low, and fluctuates frequently. It mainly develops purplish red, gray mudstone, silty mudstone, siltstone, and argillaceous siltstone [28,29]; the special lithologic section is developed in the shallow lake, a semi-deep lake environment when the lake level rises rapidly, the shallow water delta retreats in a large range, and the lake area reaches the maximum. In this period, sedimentary structures such as small wavy cross bedding, massive bedding, and horizontal bedding reflect weak hydrodynamic conditions [30]. Although the sedimentary characteristics of the upper first member of the Shahejie Formation are similar to those of the bottom sandstone member, the thicknesses of the purplish red mudstone and the silty mudstone are obviously large, which reflects the decline of the lake level and the oxidation environment of the water body (Figure 2). According to researchers' provenance analysis results for the Lixian slope [31], the lower first member of the selected wells XL5 and XL11 are formed in the shallow lake, and the semi-deep lake sedimentary environment. Under the existing well deployment, they are ideal well locations for fine-grained sedimentary rock analysis in this study.
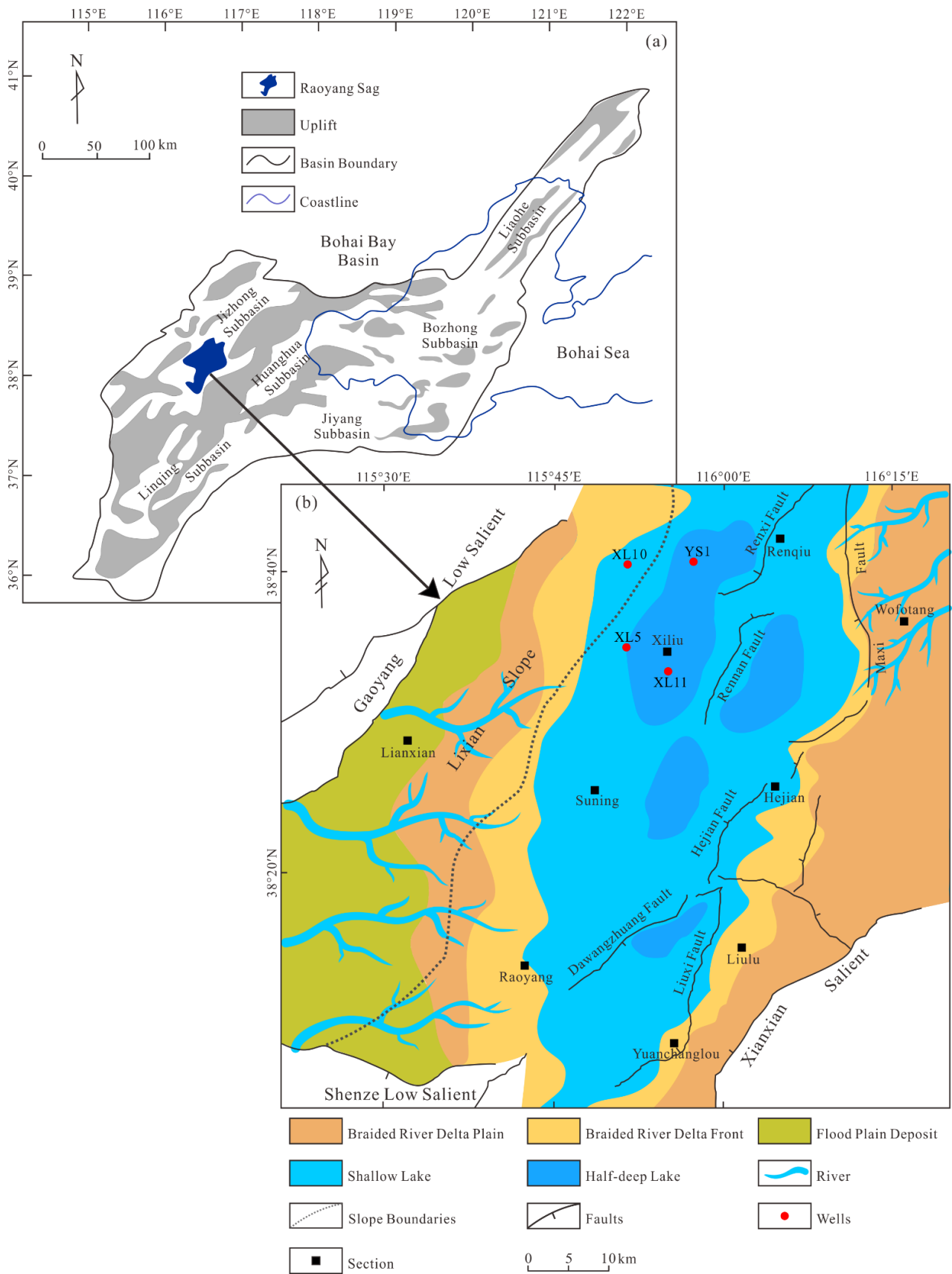
Figure 1. (**a**) Simplified structural map of Bohai Bay Basin. (**b**) Sedimentary facies distribution map of the lower first member of the Shahejie Formation (Es_1L) and key well locations of Raoyang Sag.
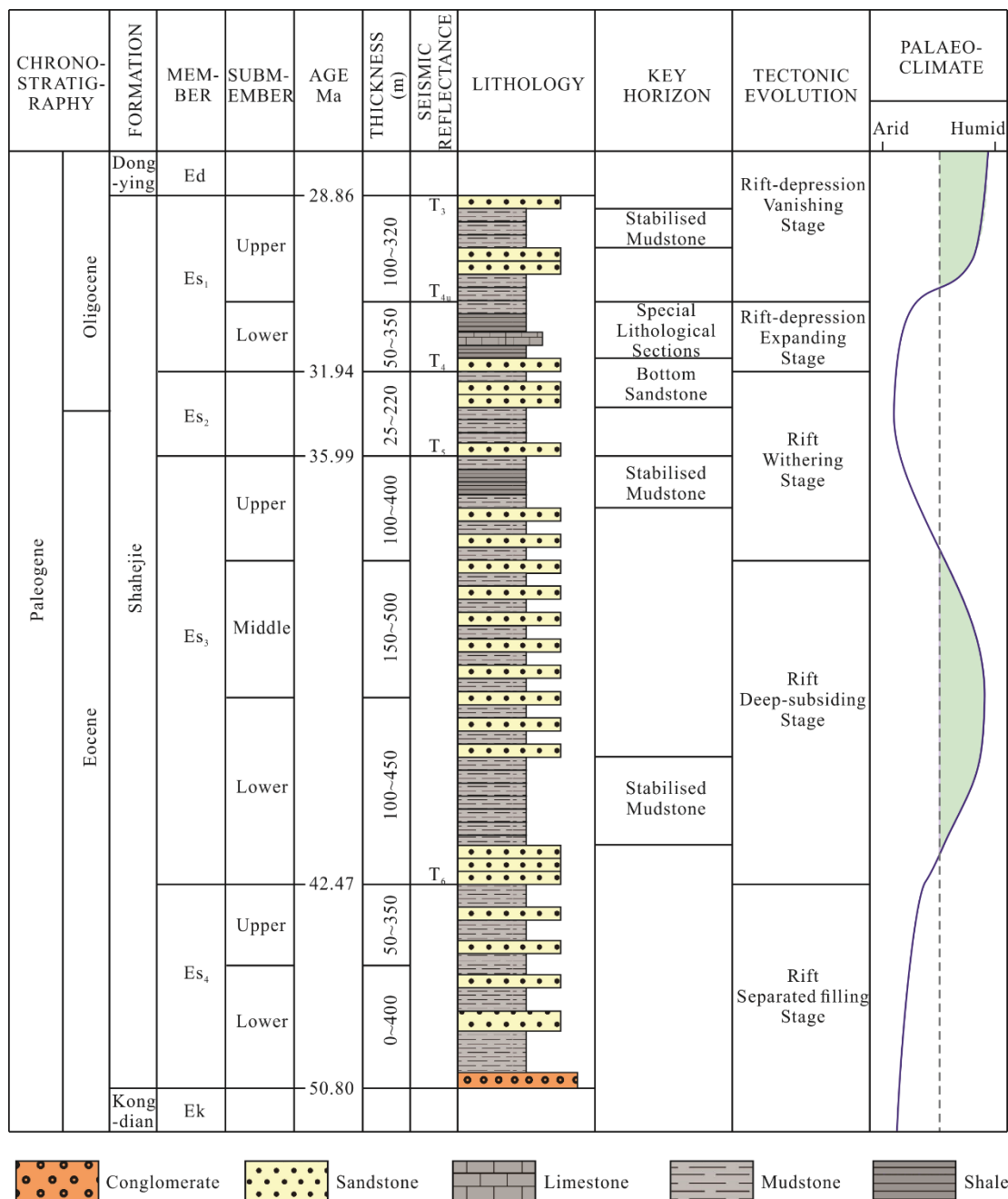
Figure 2. Stratigraphic sequence of the Shahejie Formation in Raoyang Sag.

3. Samples and Methods

3.1. Analytical Procedures

In this study, we collected 122 core samples from Es_1L in two wells in Raoyang Sag. Well XL5 is located in the Xiliu area in the northern part of the Lixian slope (106 samples, sampling depths from 3327.54 m to 3366.6 m). Well XL10 is located in the Xiliu area (14 samples, sampling depths from 3105 m to 3465 m).

The lithofacies of the source rock samples are mainly silty mixed fine-grained rock, massive clay rock, shale limestone mixed fine-grained rock, matter shale calcareous clay rock, and matter shale limestone. All samples were subjected to measurements of their total organic carbon (TOC) contents, Rock-Eval pyrolysis, and concentrations of major and trace elements (Table 1). Other portions of the samples were used for the determination of the

carbon isotope ratios of organic matter, the carbon and oxygen isotope ratios of carbonates, major and trace element concentrations, and mineral compositions (Table 2).

Table 1. Results of TOC analysis of the samples from Es_1L.

Well XL5												Well ND1	
Depth (m)	TOC (mg/g)	Depth (m)	TOC (mg/g)	Depth (m)	TOC (mg/g)	Depth (m)	TOC (mg/g)	Depth (m)	TOC (mg/g)	Depth (m)	TOC (mg/g)	Depth (m)	TOC (mg/g)
3327.54	1.13	3337.74	1.90	3344.7	1.49	3352.5	2.98	3358.9	3.48	3364.8	2.40	3075	0.86
3328.14	1.13	3338.04	2.44	3345.1	1.85	3352.9	6.33	3359.1	3.62	3365.2	2.31	3105	2.35
3328.64	1.31	3338.34	6.46	3345.4	3.80	3353.3	2.89	3359.3	3.98	3365.3	1.67	3115	2.40
3329.14	1.36	3338.74	2.98	3345.7	4.61	3353.5	2.12	3359.5	3.66	3365.8	2.58	3155	0.50
3329.57	1.45	3339.04	4.43	3346.1	6.06	3353.8	2.26	3359.7	4.56	3366.3	2.31	3185	0.86
3330.07	1.45	3339.4	2.12	3346.4	2.58	3354.2	3.62	3360	4.07	3366.6	2.12	3210	0.72
3330.75	1.31	3339.7	1.85	3346.7	2.94	3354.6	4.79	3360.3	2.17			3225	0.63
3331.05	0.95	3339.9	1.63	3347	3.62	3354.8	6.37	3361.2	2.08			3245	0.72
3331.67	1.63	3340.4	1.85	3347.4	1.18	3355.2	3.03	3361.5	4.07			3275	0.68
3332.07	1.54	3340.85	2.21	3347.7	0.99	3355.3	5.11	3361.7	2.89			3285	1.08
3333.04	1.54	3341.1	2.98	3348	1.31	3355.6	5.42	3361.9	2.71			3300	1.13
3333.39	1.45	3341.7	3.53	3348.5	2.76	3355.8	4.07	3362.1	4.93			3307.5	1.13
3333.84	1.18	3342	3.03	3349.5	2.71	3356.4	3.57	3362.4	1.13			3350	0.68
3334.64	2.08	3342.4	1.94	3349.9	4.34	3356.7	2.31	3362.7	1.90			3372	0.72
3335.44	2.12	3342.8	2.03	3350.4	2.26	3357.2	2.35	3362.9	2.12			3395	0.86
3335.94	1.76	3343	1.94	3350.8	1.90	3357.6	4.56	3363.2	1.49			3465	1.76
3336.34	1.81	3343.4	1.67	3351.1	1.72	3357.8	3.62	3363.3	2.44				
3336.74	1.81	3343.8	1.81	3351.3	1.67	3358	3.62	3363.5	2.08				
3337.04	1.58	3344.1	1.90	3351.4	1.81	3358.1	3.71	3364.3	2.89				
3337.34	1.90	3344.4	4.11	3351.8	3.80	3358.3	3.89	3364.6	2.98				

The TOC analyses and Rock-Eval pyrolysis were conducted at the Petroleum Geology Laboratory, China University of Petroleum (Beijing). The TOC determinations were performed with an elemental analyzer, LECO, model 628 CN. The samples for the determination of total organic carbon (TOC) were prepared by first decarburizing in a porous porcelain crucible using 1.0 mol/L heated hydrochloric acid to eliminate inorganic carbon, and washing with hot water for 4 h to completely remove the chlorides. Then, the treated samples were dried at 80 °C and weighed. The shale samples were analyzed using the Rock-Eval 6 instrument, weighing approximately 60–80 mg of powdered sample and testing S_{1-1} at 200 °C for 1 min, ramping up to 350 °C at 25 °C/min and ramping down to S_{1-2} for 1 min, and then ramping up to 450 °C at 25 °C/min and ramping down to S_{2-1} for 1 min, and finally ramping up to 600 °C for S_{2-2} at 25 °C/min.

The trace element analysis of samples was performed at the Institute of Uranium Mining and Geology, Beijing. Prior to measuring the major element content of the samples using an AxiosMax instrument (PANalytical), the samples were first ground to 200 mesh in an agate container, weighed to approximately 0.7 g of sample powder and 7 g of latent solvent ($Li_2B_4O_7$ + NH_4NO_3 + LiF), and stirred thoroughly in a platinum crucible. The trace element contents were determined using an Elan DRC-e ICP-MS with a temperature of 23.1 °C and a relative humidity of 42.3%. The samples were analyzed after undergoing dissolution with HF and HNO_3. The precision and accuracy of the results were better than ± 4% for major elements, and generally better than ± 2 ppm for trace elements.

Table 2. Major and trace element concentrations and some relevant parameters in Es_1L.

Well XL5														
Depth (m)	Al	Na	K	P	B	Ga	Sr	Ba	Mo	U	S_{1-1}	S_{1-2}	S_{2-1}	S_{2-2}
	(ppm)										(mg/g)			
3327.34	53,047	8807	15,152	514.00	20.02	12.8	497	655	1.3	2.5	0.06	2.06	4.46	3.29
3329.17	58,235	9230	17,301	523.95	19.78	16.2	490	677	1.0	2.3	0.08	1.95	7.52	7.42
3331.67	51,221	8792	14,040	514.77	18.41	17.4	511	869	1.5	2.3	0.11	2.13	8.88	7.29
3332.07	55,239	8918	15,575	515.26	18.32	15.6	501	673	1.9	2.8	0.10	2.47	8.57	8.35
3332.64	57,844	8977	16,056	514.68	19.34	15.2	614	678	2.0	3.2	0.15	2.22	7.20	7.82
3345.7	60,448	8651	18,844	498.87	19.58	15.0	788	675	3.4	5.2	0.24	3.24	17.32	15.94
3351.3	57,939	8985	18,380	532.12	20.09	16.1	1773	836	5.7	6.4	0.22	3.79	15.29	10.64
3352.5	35,942	7323	9758	525.86	22.01	10.2	4437	1432	9.3	6.7	0.28	4.41	17.67	18.88
3352.9	50,839	8874	16,405	522.73	20.53	11.8	2067	1159	11.7	4.9	0.25	4.91	15.11	15.41
3357.3	52,200	9512	16,148	527.67	20.41	12.6	1964	1355	11.9	5.8	0.25	4.41	18.76	25.29
3359.3	61,502	9578	19,326	524.22	20.27	16.5	1092	1120	6.0	6.3	0.40	4.79	17.91	32.67
3363.6	49,738	8332	16,870	500.90	19.84	14.3	2802	1100	3.2	4.7	0.24	4.37	20.86	16.44
3363.9	62,725	8836	21,384	520.59	18.87	16.3	777	1211	12.1	8.0	0.25	4.49	15.12	15.33
3364.1	57,849	8184	20,039	514.90	20.13	15.0	1488	1141	4.8	4.1	0.40	7.66	20.03	18.40
Well ND1														
Depth (m)	Al	Na	K	P	B	Ga	Sr	Ba	Mo	U				
	(ppm)													
3075	60,600	11,800	21,900	740	23.4	21.6	853	745	0.9	3.1				
3105	51,300	9490	19,200	664	26.2	18.6	820	772	1.5	3.4				
3115	57,000	9930	21,200	607	20.7	20.2	1080	688	1.4	3.4				
3155	59,500	12,000	23,600	685	20.3	21.6	343	686	0.8	2.6				
3185	58,900	10,700	23,500	796	21.3	21.5	366	760	0.9	2.7				
3210	72,100	8500	25,600	829	24.5	25.9	943	983	1.1	3.2				
3225	58,400	12,600	23,400	737	18	21.3	347	746	1.2	2.4				
3245	55,400	11,400	21,800	658	28.8	20.4	379	631	0.9	2.6				
3275	59,800	12,400	22,900	706	27.1	21.2	439	680	0.7	2.8				
3285	46,500	8620	20,600	462	26.6	16.1	940	693	2	2.8				
3300	56,800	10,100	20,200	694	20.5	20.3	1410	857	1.8	2.3				
3307.5	57,200	12,200	22,400	735	16.4	20.3	597	735	1.5	2.2				
3350	61,000	12,400	25,300	687	24.5	22.2	417	708	0.8	2.9				
3372	62,100	14,500	22,200	790	19.3	22.3	254	930	1	2.4				
3395	55,300	9230	22,100	677	18.8	20.1	929	950	1.2	2.4				
3465	54,300	10,300	23,100	427	54.3	18.8	995	879	1.8	2.8				

3.2. Proxy Calculations

The determination of selected trace elements allows the calculation of CIA (Chemical Alteration Index) values, organic phosphorus (Porg), and enrichment factors for Mo and U to assess the chemical weathering, paleoproductivity, and redox conditions in the lake basin [32–38]. It has been suggested that CaO should be excluded from the original CIA equation of Nesbitt and Young (1982) because it is difficult to accurately determine the CaO values derived from carbonates in calcareous sedimentary rocks. Therefore, we used a modified equation of CIA*, as follows [39]:

$$CIA^* = [Al_2O_3/(Al_2O_3 + Na_2O + K_2O)] \times 100 \tag{1}$$

We also used $Ln(Al_2O_3/Na_2O)$ as a weathering index to corroborate the CIA*.

We used total phosphorus (Ptotal) minus the fraction of detrital phosphorus (Pdetr) estimated from the Al contents of each sample to calculate Porg, using the following equation.

$$Porg = Ptotal - Al \times (P/Al)detr \tag{2}$$

We also assumed a rock chip P/Al ratio of 0.0062 based on the P and Al concentrations of continental crust and rocks in eastern China [40].

To compare Mo and U enrichments in different areas of the study area, this is expressed in the form of enrichment factors (EFs), which are calculated as follows:

$$EF_X = (X/Al)sample/(X/Al)PAAS \qquad (3)$$

The samples were normalized by the average composition of the Post Tertiary Australian Shale (PAAS). These enrichment factors reflect the autochthonous trace element concentrations in the samples relative to those in the average shale. In practice, a relative enrichment corresponds to $EF_X > 1$ and an abundant enrichment corresponds to $EF_X > 3$. If $EF_X < 1$, then the element X is depleted.

4. Results and Discussion

4.1. Lithofacies Division and Petrological Characteristics

Through X-ray diffraction experimental analysis, the samples taken from wells XL5 and XL11 in the northern Lixian slope are analyzed. The data statistics show that the fine-grained sedimentary rocks in this area mainly include carbonate minerals, clay minerals, quartz, and feldspar; the carbonate minerals are mainly calcite, with an average of 23.7% and a maximum of 47%; the content of clay minerals is less than 50%, and most of them are between 30% and 50%. The average content of quartz is 17%, and the highest is 26%. In addition, the TOC of the samples in this area was tested by rock pyrolysis: the TOC content was mostly higher than 1%, and some even reached 14%. In this study area, the results of the mineral composition reflecting the content of carbonate are negatively correlated with those of clay and quartz, respectively (Figure 3). This phenomenon is due to the fact that clay minerals, quartz, and feldspar are formed by physical factors such as weathering and transportation, while carbonate minerals are formed by chemical factors in the basin.
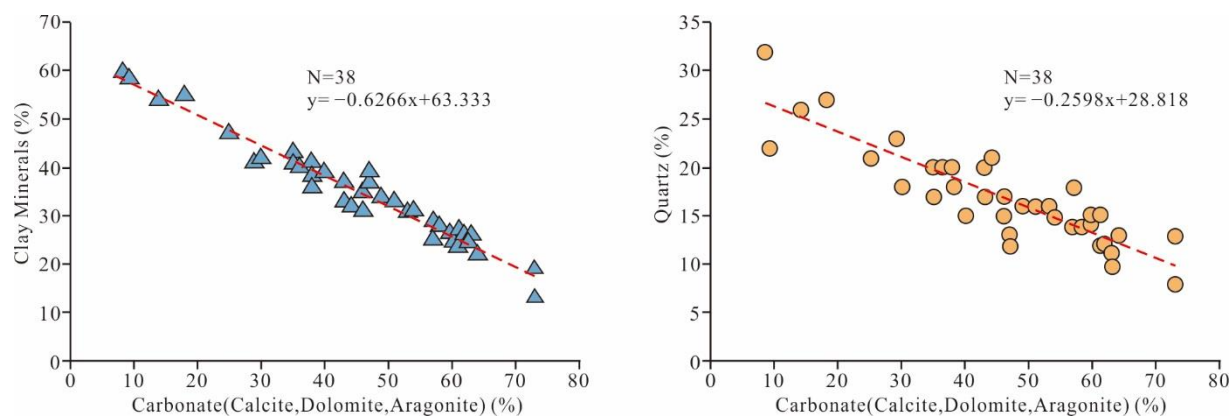

Figure 3. Interrelation of carbonate rocks, quartz, and clay minerals in fine-grained sedimentary rocks of Es$_1$L in the Xiliu area, Raoyang Sag.

The lithofacies description includes the differences between the mineral compositions. According to the structural characteristics of the samples, clay, quartz feldspar, and carbonate are used as the three end elements, and a content of 50% is used to divide them into three categories: clay rock, carbonate rock, and mixed fine-grained rock. Combined with the typical sedimentary structural characteristics, the shale section of Es$_1$L is divided into five lithofacies: silty mixed fine-grained rock, shale limestone mixed fine-grained rock, massive clay rock, shale clay rock, and shale limestone. The comparison of organic matter abundance of the above lithofacies shows that the organic matter enrichment characteristics of different lithofacies are obviously different (Figure 4). The development of lamellation and the increase in carbonate content are accompanied by the enrichment of organic matter. Combined with the abundance of organic matter, the lithofacies of fine-grained sedimen-

tary rocks in the target section are divided into five types: medium organic silty mixed fine-grained rock, high organic shale limestone mixed fine-grained rock, medium organic massive clay rock, high organic shale clay rock, and high organic shale limestone (Figure 5).
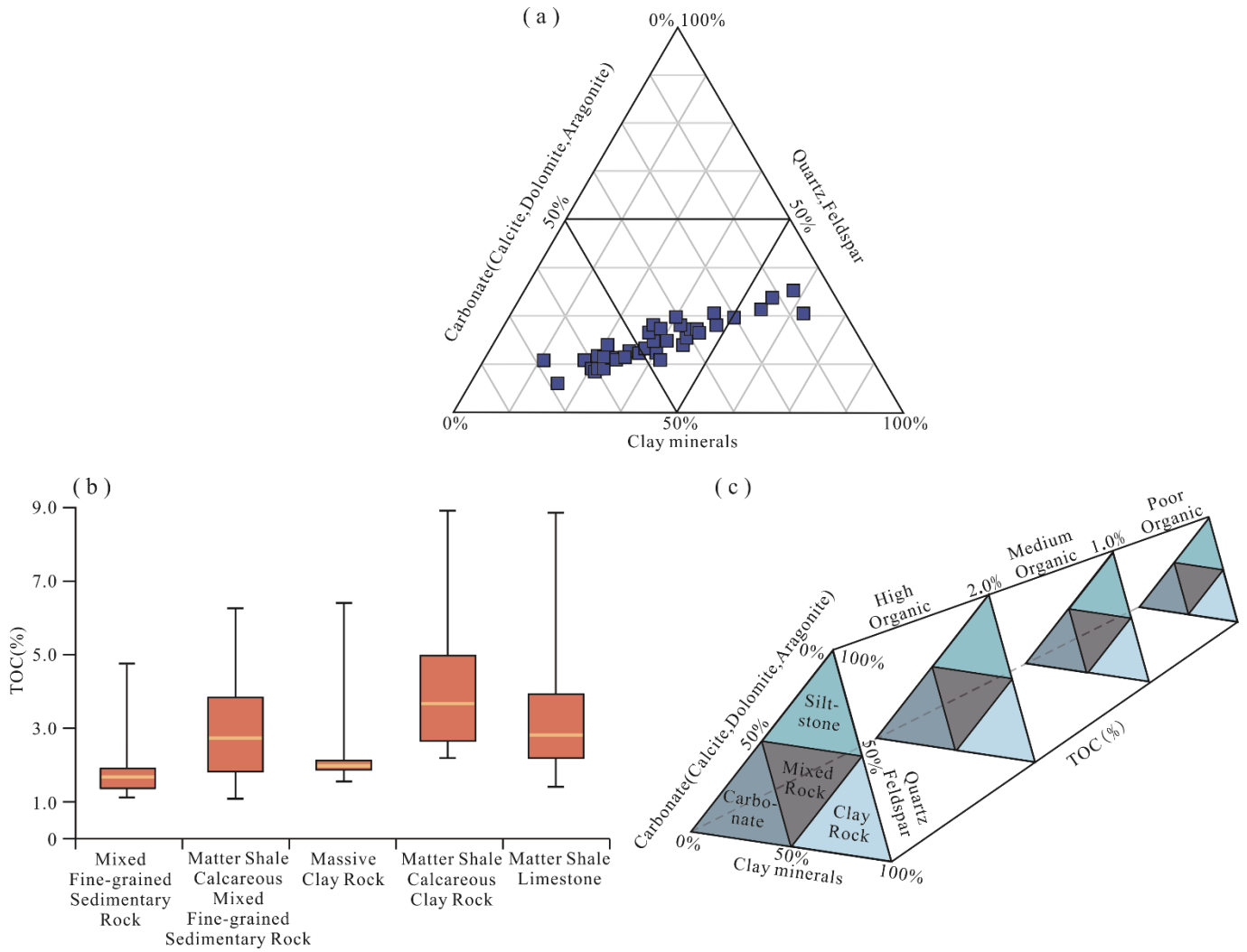

Figure 4. Mineral content characteristics, organic matter abundance, and lithofacies classification of Es$_1$L in the Xiliu area. (**a**) X-ray diffraction mineral content of whole rock; (**b**) Abundance characteristics of organic matter in different lithofacies; (**c**) Lithofacies division scheme.

LITHOFACIES	AVERAGE MINERAL CONTENT	TOC (%) 1% 3%	MACROSCOPIC FEATURES (ROCK CORES)	MICROSCOPIC FEATURES	
Medium Organic Silty Mixed Fine-grained Sedimentary Rock	Carbonate 26% Clay minerals 34% Quartz 26% Feldspar 14%				
Medium Organic Massive Clay Rock	Carbonate 14% Clay minerals 54% Quartz 26% Feldspar 6%				
High Organic Matter Shale Calcareous Mixed Fine-grained Sedimentary Rock	Carbonate 35% Clay minerals 41% Quartz 17% Feldspar 4%				
High Organic Matter Shale Calcareous Clay Rock	Carbonate 23% Clay minerals 52% Quartz 21% Feldspar 4%				
High Organic Matter Shale Limestone	Carbonate 63% Clay minerals 25% Quartz 11% Feldspar 1%				
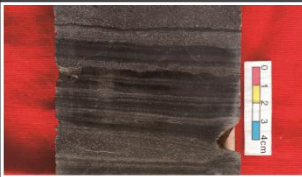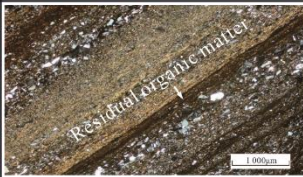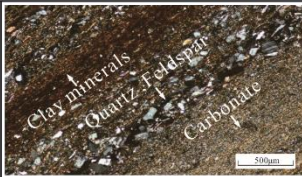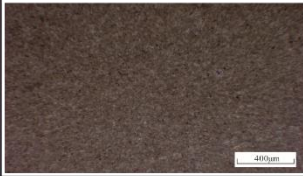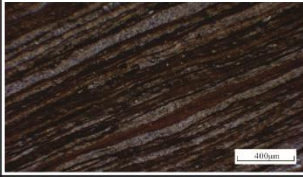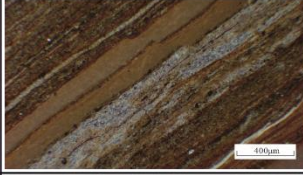
Figure 5. Lithofacies classification scheme of Es_1L in the Xiliu area, Raoyang Sag.

4.1.1. Medium Organic Silty Mixed Fine-Grained Sedimentary Rock

The lithology-core section is presented in gray, and horizontal sand grain bedding is present (Figure 6a). Thin section analysis reveals that for the argillaceous bedding structure, clay minerals alternate with quartz and feldspar, the long axes of sandy debris are directional, and the clastic suspension is in the argillaceous layer (Figure 6b,c). Dolomite and calcite are in the finest argillaceous mixed crystalline form, and in black layered organic residual strips. The clay mineral content is less than 40%, and the recrystallization shows directionality. Small amounts of iron minerals are distributed as spots. The porosity of the rock is not well developed, and unfilled microfractures with a width of about 0.01 mm are occasionally seen. These characteristics indicate that this type of lithofacies may be developed in shallow lake sediments with a reduced reduction environment and hydrodynamic conditions. However, the terrigenous supply in the north of the slope accounts to high quartz and less organic matter.
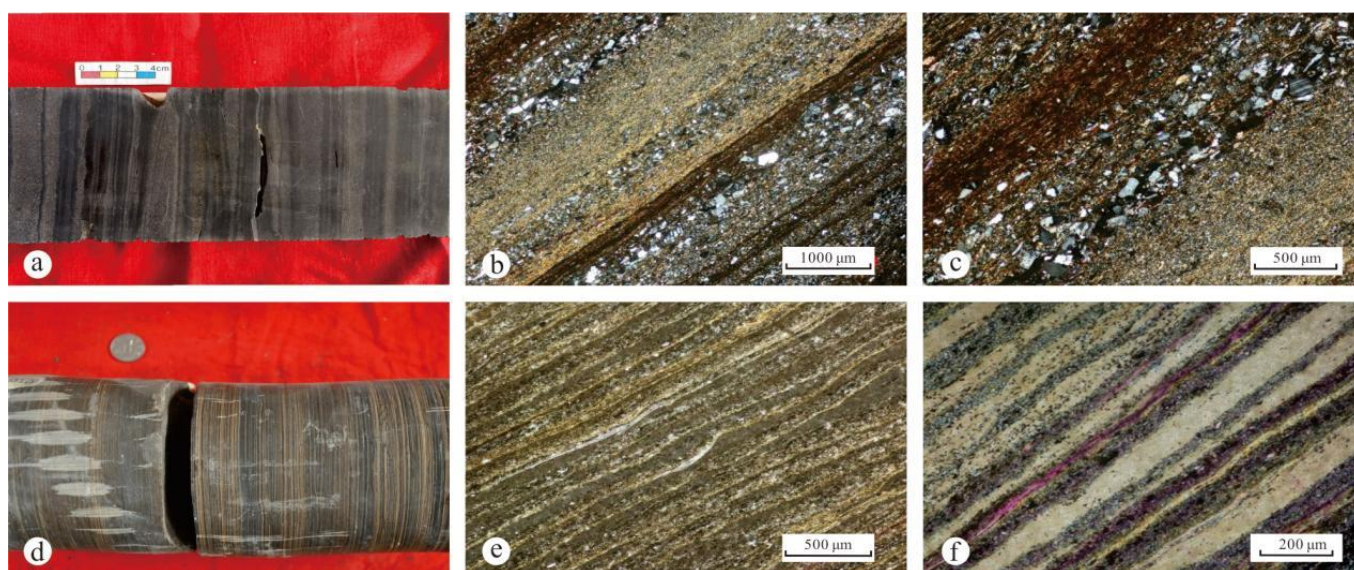
Figure 6. (**a**) Silty mixed fine-grained sedimentary rock core, Well XL5, 3320 m; (**b**) laminated structure of shale, interbedding of clay layer and carbonate layer, visible quartz feldspar grains (+), Well XL5, 3320.2 m; (**c**) laminated structure of shale, visible black residual organic matter (+), Well XL5, 3320.2 m; (**d**) calcareous mixed fine-grained sedimentary rock, Well XL5, 3355 m; (**e**) interbedding of clay layer and carbonate layer, organic matter laminar distribution (−), Well XL5, 3355.6 m; (**f**) laminated structure of shale, organic matter laminar distribution (+), Well XL5, 3355.6 m.

4.1.2. High Organic Matter Shale Calcareous Mixed Fine-Grained Sedimentary Rock

The core samples are gray/dark gray and laminated (Figure 6d). Thin section microscopy shows that pelitic texture, laminar argillaceous stripes, and carbonate stripes are distributed alternately. Micritic calcite, abundant clay minerals, dark organic laminae, and a small amount of quartz and feldspar particles were observed in the thin sections. In terms of composition, the clay content is 35%–43%, the calcite content is 30%–40%, and the quartz and feldspar contents are 15%–25%; the TOC is generally 1.2%–4%, with an average of 2.9%, and without dominant components (Figure 6e,f). Punctate iron is present, with a content of 4.5%, distributed in the argillaceous layer. Diagenetic fractures are about 0.01 mm. Pyrite is recorded. This result displays that the samples may be formed in a semi-deep lake with a strong reduction environment. The effect of the hydrodynamic conditions is far less than that in the sedimentary environment of silty mixed fine-grained rocks. The interference of sediment provenance is significantly reduced and the stable water environment causes the lamellation to be highly developed.

4.1.3. Medium Organic Massive Clay Rock

The gray-colored massive structure is presented in Figure 7a. According to the thin-section microscopy, the laminae are not developed, and the main composition is clay minerals, some of which are recrystallized (Figure 7b,c). The clay mineral content is 50%–58%, the carbonate content dominated by micritic calcite is 10%–20%, the quartz and feldspar contents are 30%–40%, the quartz is distributed sporadically, and the lenticular siliceous body is rare. The TOC content ranges from 1.5% to 2.0%, and the content of iron minerals is 2.5%, which are dominantly distributed punctate, and some are clustered into stripes and patches. The micrite calcite stripes and the laminar distribution of black organic matter are rare. The diagenetic fractures are basically undeveloped. It is comprehensively advocated that the effect of the environmental hydrodynamic conditions of this type of lithofacies are strong, the content of pyrite is low, and the environmental reducibility is not strong, showing that it may be formed in a shallow lake sedimentary environment.
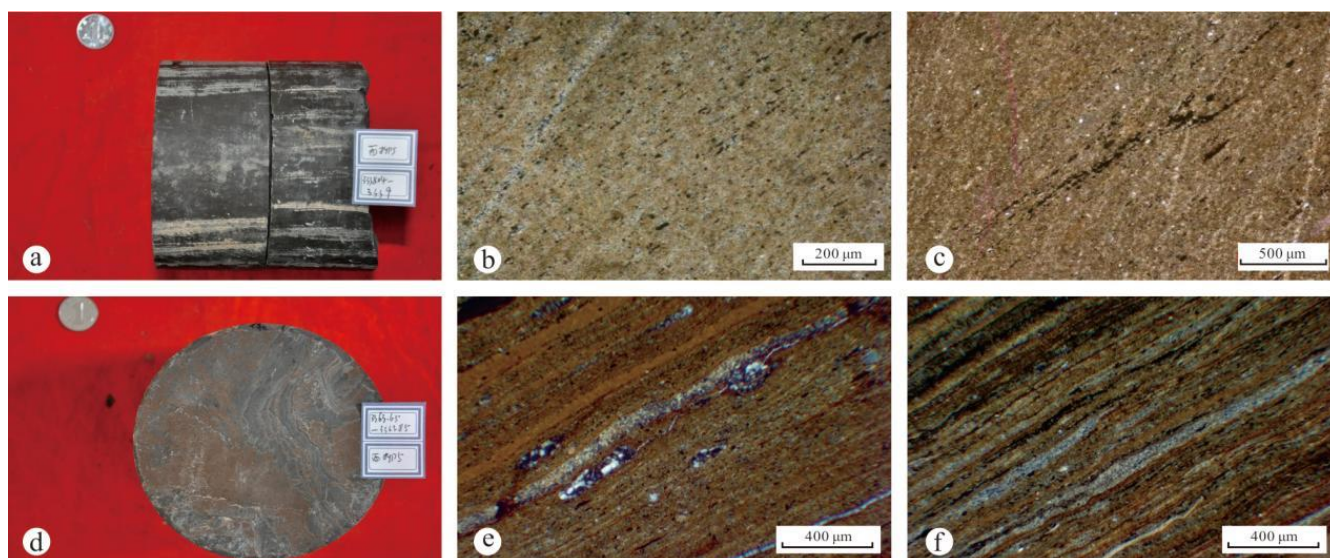
Figure 7. (**a**) Massive clay rock core, Well XL5, 3338 m; (**b**) massive structure, extensive clay and minor carbonate minerals seen, organic matter punctate distribution (−), Well XL5, 3338.74 m; (**c**) massive structure, extensive clay and carbonate minerals seen (+), Well XL5, 3338.74 m; (**d**) matter shale calcareous clay rock core, Well XL5, 3363.9 m; (**e**) small amount of calcite streaks, visible silicon lens body, laminated structure of shale (+), Well XL5, 3363.9 m; (**f**) striped distribution of organic matter, calcite streaks, laminated structure of shale (+), Well XL5, 3363.9 m.

4.1.4. High Organic Matter Shale Calcareous Clay Rock

The core sample is black gray, and the lamellation is very developed. The thin section shows that this lithofacies is dominated by clay minerals, with fewer carbonate minerals. Black lamellar organic matter enrichment, a small amount of lamellar quartz feldspar, and generally developed pyrite can be observed through thin sections (Figure 7e,f). In terms of composition, the total content of clay minerals is 51%–58%. The carbonate mineral content is distributed from 8% to 23%, the content of quartz and feldspar is 20%–23%, and the TOC content is between 2% and 6.5%, with an average content of 3.6%. These data imply that this type of rock was formed in a lake environment with a deep water body and strong reducibility, with weak hydrodynamic conditions, and a large amount of organic matter preserved.

4.1.5. High Organic Matter Shale Limestone

The core sample is dark gray/ash black, and the lamellation is well developed (Figure 8a). The thin sections show clay mineral laminae interbedded with carbonate laminae frequently, and the black organic laminae are well developed (Figure 8b,c). The carbonate laminae are dominantly composed of micritic calcite and a small amount of pyrite, and the thickness is obviously larger than that of clay mineral laminae (Figure 8e,f). Quartz feldspar particles and bioclasts are occasionally observed. In terms of the composition, the clay content is 10%–25%, the carbonate mineral content is more than 50%, the quartz and feldspar contents are less than 10%, and the TOC content is 2.1%–6.7%, with an average of 3%. These characteristics indicate that this type of lithofacies may be formed in a deep-water environment, and the water body is highly reductive and rarely affected by the terrestrial organic matter supply.
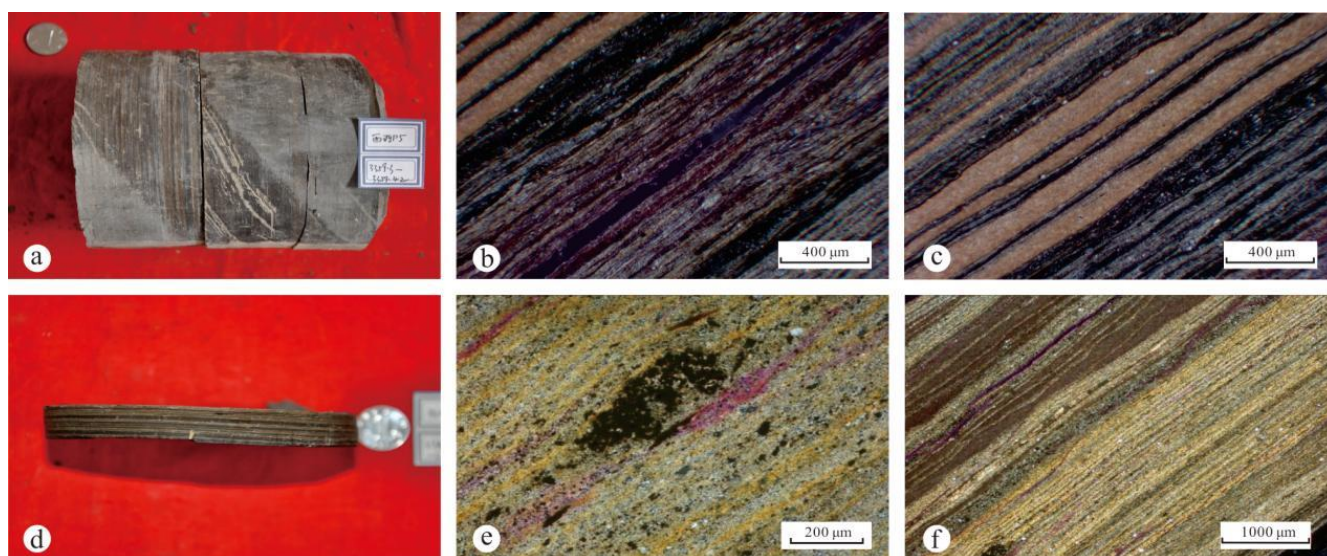
Figure 8. (**a**) Matter shale limestone core, Well XL5, 3359.3 m; (**b**) interbedded clay and calcite (−), Well XL5, 3359.3 m; (**c**) the thickness of micrite calcite is greater than that of clay layer, clear lamina (−), Well XL5, 3352.9 m; (**d**) matter shale limestone core, Well XL11, 3420 m; (**e**) micrite calcite, visible point iron minerals (+), Well XL11, 3420.92 m; (**f**) clay layers interbedded with cryptocrystalline calcite, organic matter laminar distribution (+), Well XL11, 3420.92 m.

4.2. Geological Significance of Fine-Grained Lithofacies

4.2.1. Occurrence of Organic Matter

Comparing the five lithofacies types, the lithofacies with well-developed lamellation have abundant lamina of organic matter, resulting in a high organic matter content. Scanning electron microscopy shows that the primary organic matter is dominantly interbedded with clay minerals and carbonate minerals in strips (Figure 9a–c), and can also be mixed in carbonate minerals and clay minerals in bulk form. Dissolution fractures are rare, but organic matter pores are ill-developed (Figure 9d–f). For silty mixed fine-grained rocks with undeveloped lamellation, abundant authigenic quartz and pyrite are reported (Figure 9g–i). The primary organic matter is distributed in a spherical shape, and the organic matter pores are basically undeveloped (Figure 9j). The primary organic matter individuals in the massive clay rock are small and are distributed in a scattered manner (Figure 9k,l). Multi-temperature pyrolysis is used to examine the organic matter abundance of different lithofacies in Es_1L: S_{1-1} (hydrocarbon content in unit rock is detected at 200 °C, free state), S_{1-2} (hydrocarbon content in unit rock is detected at 200–350 °C, free state), S_{2-1} (hydrocarbon content in unit rock is detected at 350–450 °C, adsorbed or bound state), and S_{2-2} (kerogen pyrolysis hydrocarbon generation component). The results show that the amount of free and adsorbed hydrocarbons in the shale limestone mixed fine-grained rock, shale clay rock, and shale limestone are significantly higher than those in massive clay rock and silty mixed fine-grained rock, and that the amounts of free and adsorbed hydrocarbons in silty mixed fine-grained rock are the lowest (Figure 10). This indicates that the development of lamellation is conducive to the occurrence of a large amount of organic matter and is rich in free-phase hydrocarbons. Therefore, the change of sedimentary environment between different rocks leads to the difference of mineral composition and the occurrence of organic matter. The evaluation of shale organic matter should be based on the type of lithofacies and the dominant facies should be established to eliminate the uncertainty of the overall evaluation with the parameters of hydrocarbon generation potential ($S_1 + S_2$).
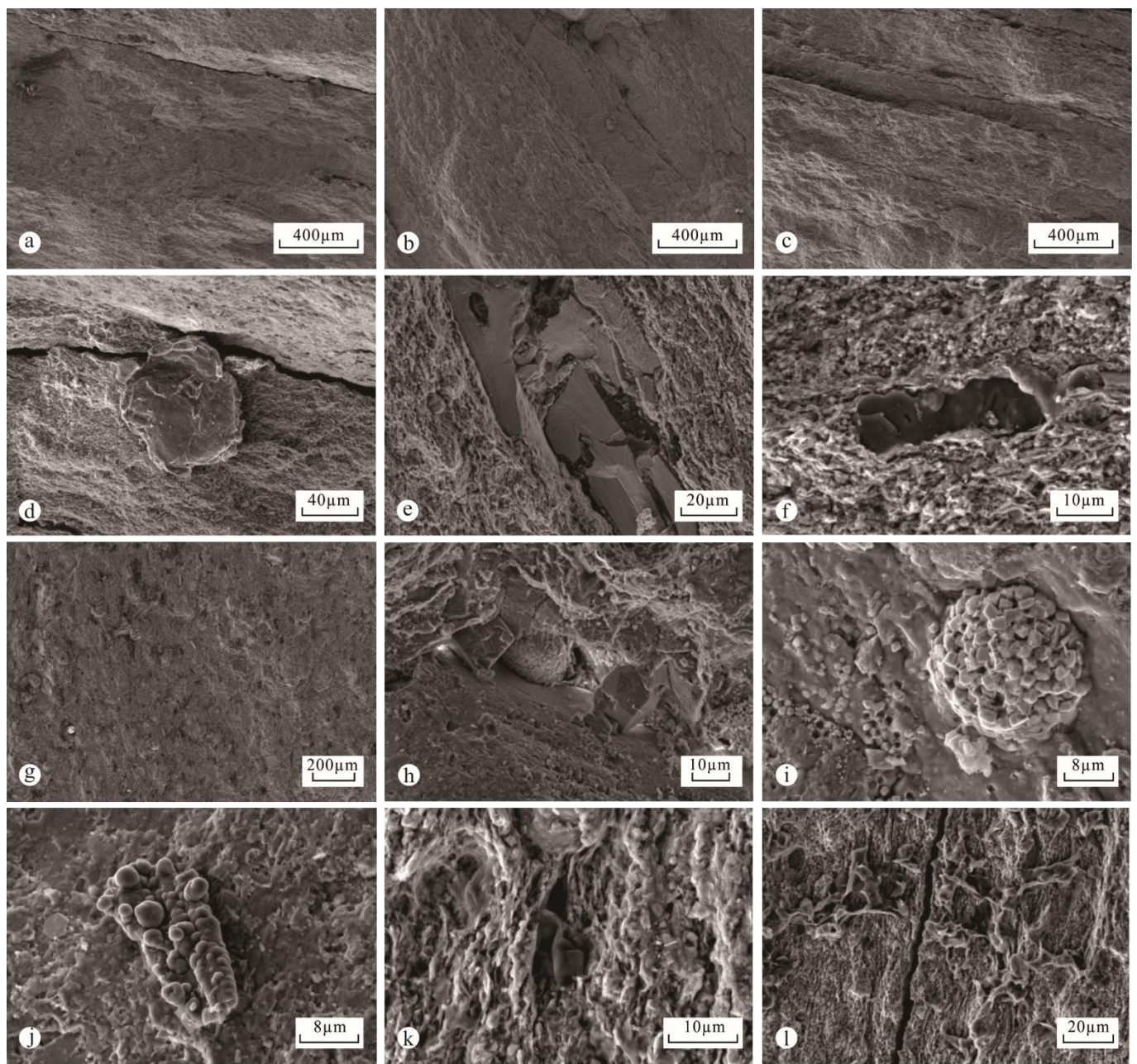
Figure 9. SEM characteristics of fine-grained rocks in the lower first member of the Shahejie Formation in the Xiliu area of Raoyang Sag. (**a**) High organic matter shale limestone, Well XL11, 3351.3 m; (**b**) high organic matter shale limestone, Well XL5, 3360.82 m; (**c**) high organic matter shale calcareous clay rock, Well XL5, 3346.1 m; (**d**) organic matter developed between laminae, Well XL11, 3351.3 m; (**e**) carbonate minerals intercalated with organic matter, Well XL5, 3360.82 m; (**f**) clay minerals intercalated with organic matter, Well XL5, 3346.1 m; (**g**) medium organic silty mixed fine-grained sedimentary rock, Well XL5, 3328.5 m; (**h**) intergranularly developed pyrite and autochthonous quartz, Well XL5, 3328.5 m; (**i**) intercrystalline development of strawberry pyrite, Well XL5, 3328.5 m; (**j**) spherical organic matter, Well XL5, 3328.5 m; (**k**) small organic matter developed in clay minerals, Well XL5, 3332.64 m; (**l**) scattered organic matter, Well XL5, 3332.64 m.
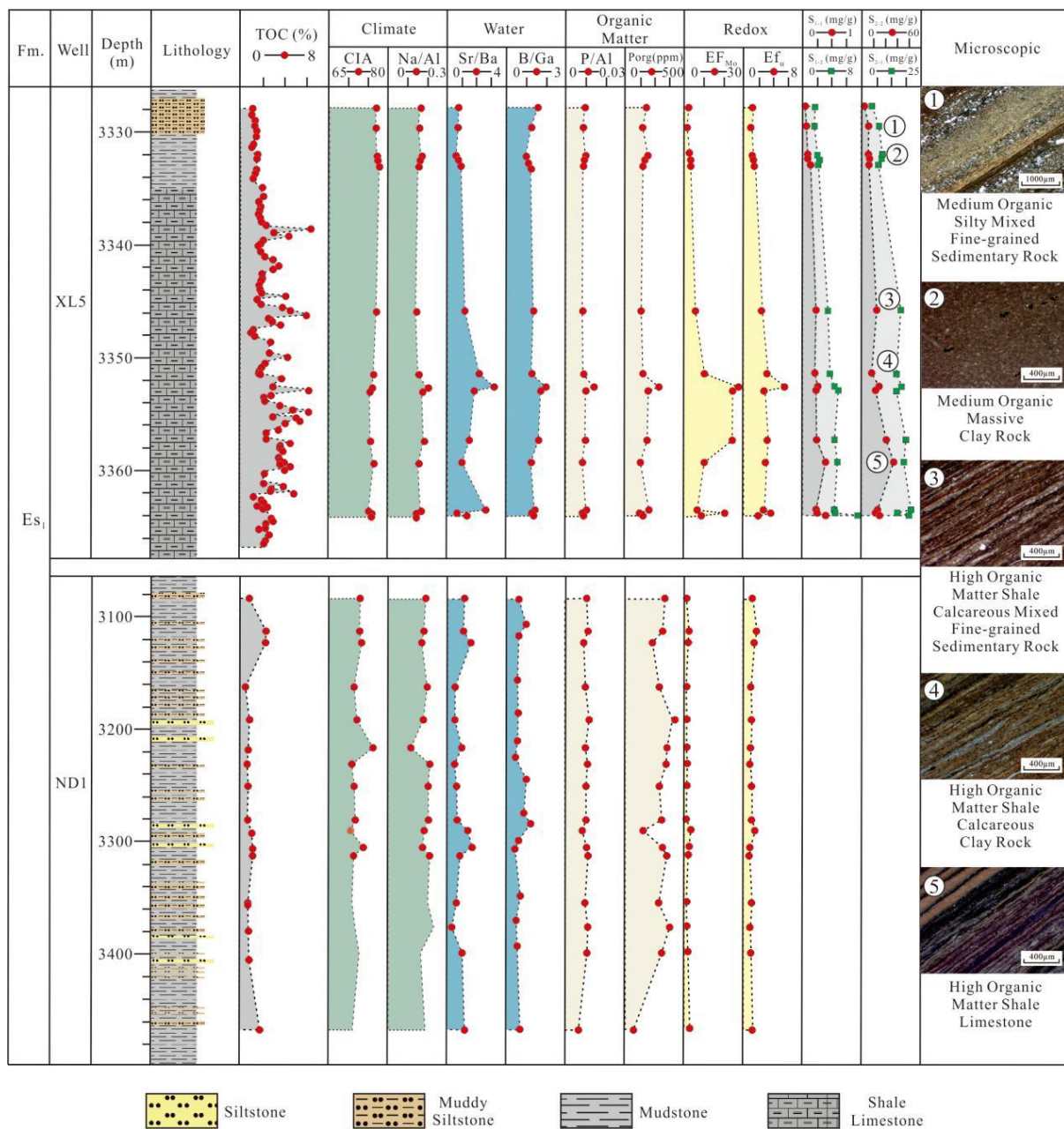
Figure 10. Lithofacies sedimentary environment and occurrence state of organic matter of fine-grained rocks in the lower first member of the Shahejie Formation in the Xiliu area of Raoyang Sag.

4.2.2. Sedimentary Environment

Based on the element analysis of the core samples, the main indicators for the environment judgment in this study are: Na/Al and CIA (chemical index of alteration) [41,42], trace elements Sr/Ba, B/Ga [43], major element ratio P/Al [44], organic autogenous phosphorus (Porg), and enrichment factor of redox sensitive elements Mo and U (EFmo, EFu). Though the comprehensive geochemical evaluation of samples of a drilled-well XL5 in the Lixian slope is relatively dense, the vertical changes of various sedimentary environmental indicators are small, among which Sr/Ba, B/Ga, representing the salinity of the water body, and Mo and U enrichment factors, representing the redox environment of the water body, have a certain trend. In the interbedded section of argillaceous silt, and silty mudstone and mudstone, the salinity of the sedimentary water is low with low reducibility. The salinity of the shale section is obviously high, and the water body has strong reduction characteristics. The climate and organic matter productivity indicators of the water body basically do not

change much vertically, indicating that the climate and sedimentary environment are relatively stable. By comparing the relevant parameters of well ND1, a hydrocarbon source rock evaluation well in Baxian Sag in the north of the study area, the authors find a significant change trend. The mudstone of Well ND1 was formed in a sedimentary environment with high organic matter productivity in a freshwater shallow lake. The organic matter content is significantly lower than that in the Xiliu area on the northern Lixian slope, and the CIA in the Xiliu area is higher, indicating that the chemical weathering is enhanced relative to the lakes in Baxian Sag. The relatively low Na/Al value also verifies this: compared with Baxian Sag, the lake water body in the Xiliu area has the obvious characteristics of brackish water and saline water, but its organic matter productivity is lower than that of Baxian Sag, which also conforms to the characteristics of common saline water lakes. More importantly, the lake water in the Xiliu area has obvious strong reduction characteristics. As the two key wells belong to Jizhong Sag, there is no great difference in the climate background, and the difference in CIA is mainly caused by the change of water depth. The difference in water quality is mainly due to the influence of material source and sedimentary facies. Well ND1 is greatly affected by a terrigenous material supply and the water body is shallow, showing the characteristics of an open lake with a weak reduction in fresh water. Well XL5 is far from the material source and the water body is obviously deep; the hydrodynamic force is weakened. Under the dry climate background of Es_1L in Jizhong Sag, a closed lake with a strong reduction in salt water may be formed, and thus, a set of medium-high organic fine-grained rocks is developed.

The climate change in the Xiliu area of the northern Lixian slope in Raoyang Sag, mainly divided into two stages, is small during the deposition of Es_1L. The first stage is the deposition of the lower part. Although the overall climate is relatively dry, the lake is deep due to the maximum lake transgression period when the land-based input is low, the impact of material source interference is less, the water salinity is high, the chemical weathering is strong, and the salinity stratification can be formed at the bottom of the lake water body. This stage is conducive to the deposition of carbonate and the development of lamellation, mainly composed of shale limestone, shale calcareous clay rock, and shale calcareous mixed fine-grained rock. At the same time, due to obvious stratification, the water body at the bottom is highly reductive, and the redox sensitive elements Mo and U are obviously enriched; thus, the abundance of organic matter in this sedimentary stage is obviously high. The second stage is the deposition of the upper part. At this time, the overall climate is slightly humid, the main material supply of the Lixian slope is enhanced, the lake water body becomes shallow, the salinity of the sedimentary water body is significantly reduced due to the influence of the land source, and the salinity stratification of the water body is destroyed. The two lithofacies are mainly massive clay rock and silty mixed fine-grained rock, and the reducibility of the water body at the bottom of the lake is significantly reduced. In this stage, the organic matter content of sedimentary facies is generally lower than 2% (Figure 11).

Through the analysis of the experimental data of various samples, it can be found that the sedimentary environment of fine-grained sedimentary rocks is not a simple, deep-water, quiet environment. Generally speaking, when the land supply is low, the influence of the material source is less, the salinity of water body is high and the cation sufficient, and the biochemical activities increase the deposition of a large amount of endogenous carbonate, where it is easy to form high organic matter shale limestone and high organic matter shale limestone lithofacies. The micrite calcite layer, clay minerals, and organic matter laminae appear alternately under the influence of the seasons. The organic matter productivity of the surface water body is medium, and the strong reduction characteristics of the lake bottom are the key factors for the preservation of organic matter; however, in a relatively humid environment, shallow lakes are easily affected by the slope material supply, the salinity of the lake water body decreases, the chemical stratification is disturbed and destroyed, and the bulk clay rock lithofacies becomes significant. When the land source supply increases and is affected by intermittent water flow, mixed fine-grained rocks with

silty lamina will be developed. Because the overall organic matter productivities of the lakes in the Xiliu area were medium during the deposition period of Es$_1$L, the organic matter content was significantly reduced when the strong reducing environment at the bottom of the lake was destroyed.
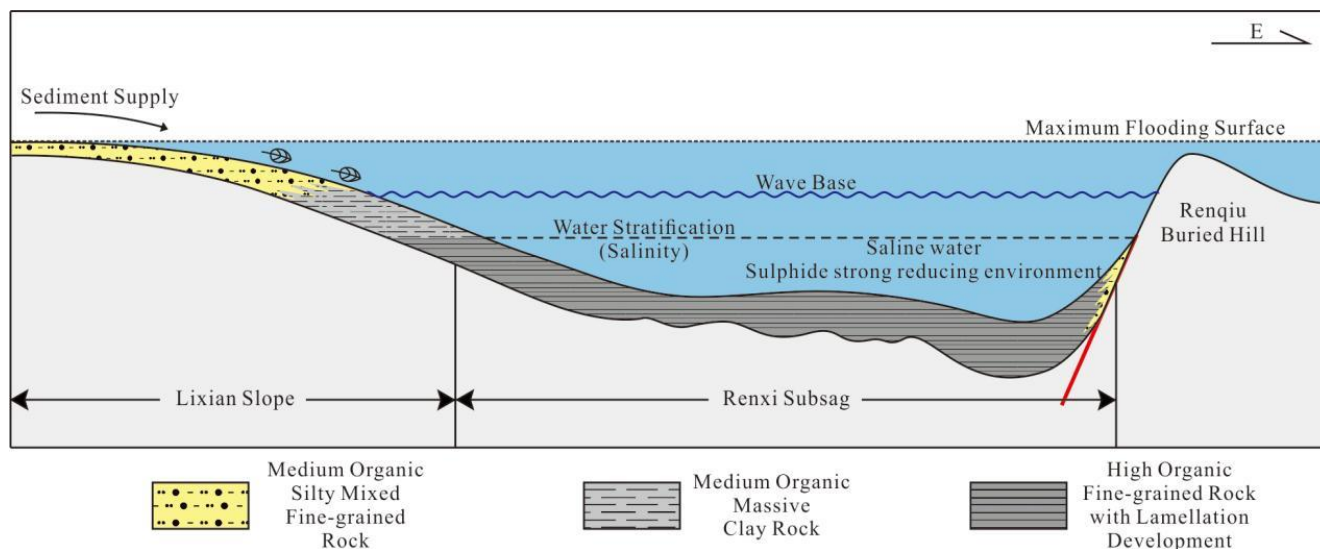

Figure 11. Lithofacies development environment model of fine-grained rocks in the lower first member of the Shahejie Formation in the Xiliu area of Raoyang Sag.

5. Conclusions

(1) Based on the mineral component, primary sedimentary structure, and organic matter abundance parameters, the fine-grained sedimentary rocks of Es$_1$L in the Xiliu area of the northern Lixian slope in Raoyang Sag are divided into five lithofacies types: medium organic silty mixed fine-grained rock, medium organic massive clay rock, high organic shale limestone mixed fine-grained rock, high organic matter shale calcareous clay rock, and high organic matter shale limestone, among which high organic matter shale limestone and high organic matter shale calcareous mixed fine-grained rock are well developed.

(2) Among the three lithofacies with lamellation, organic matter is mainly enriched in the mineral laminae in stripes, the organic matter pores are not developed, and the amounts of free hydrocarbon and adsorbed hydrocarbon have advantages; medium organic silty mixed fine-grained rock and medium organic massive clay rock with undeveloped lamellation are characterized by small-scale organic matter scattered in a disordered manner, with significantly low free hydrocarbon content and no organic matter pores.

(3) The sedimentary environment evolution of Es$_1$L in the Xiliu area of northern Lixian slope experiences different stages. At the bottom, the development of three high organic matter lithofacies is influenced by a low material source, high water salinity, and a strong reduction environment; in the upper part, the development of medium organic silty mixed fine-grained rock and medium organic massive clay rock facies is influenced by the higher material source, lower water salinity, and a weaker reduction environment.

Author Contributions: Writing—original draft, Y.L. and J.Y.; Writing—review and editing J.Y. and Z.W. All authors have read and agreed to the published version of the manuscript.

Conflicts of Interest: The authors declare no conflict of interest.

References

1. Lazar, O.R.; Bohacs, K.M.; Macquaker, J.H.; Schieber, J.; Demko, T.M. Capturing Key Attributes of Fine-Grained Sedimentary Rocks in Outcrops, Cores, and Thin Sections: Nomenclature and Description Guidelines. *J. Sediment. Res.* **2015**, *85*, 230–246. [CrossRef]
2. Milliken, K. A compositional classification for grain assemblages in fine-grained sediments and sedimentary rocks. *J. Sediment. Res.* **2014**, *84*, 1185–1199.
3. Krumbein, W.C. The mechanical analysis of fine-grained sediments. *J. Sediment. Res.* **1932**, *2*, 140–149.
4. Schieber, J.; Zimmerle, W. The history and promise of shale research. *Shales Mudstones* **1998**, *1*, 1–10.
5. Macquaker, J.H.; Adams, A.E. Maximizing information from fine-grained sedimentary rocks: An inclusive nomenclature for mudstones. *J. Sediment. Res.* **2003**, *73*, 735–744. [CrossRef]
6. Aplin, A.C.; Macquaker, J.H. Mudstone diversity: Origin and implications for source, seal, and reservoir properties in petroleum systems. *AAPG Bull.* **2011**, *95*, 2031–2059.
7. Xiong, T.; Chen, L.; Chen, X.; Ji, Y.B.; Wu, P.J.; Hu, Y.; Wang, G.X.; Peng, H. Characteristics, genetic mechanism of marine shale laminae and its significance of shale gas accumulation. *J. Cent. South Univ. (Sci. Technol.)* **2022**, *53*, 3490–3508.
8. Hao, F.; Zhou, X.; Zhu, Y.; Yang, Y. Lacustrine source rock deposition in response to co-evolution of environments and organisms controlled by tectonic subsidence and climate, Bohai Bay Basin, China. *Org. Geochem.* **2011**, *42*, 323–339. [CrossRef]
9. Huang, Q.; Chen, R.T.; Peng, X.B.; Li, X.Q.; Wang, N. Characteristics and geological significance of biomarkers from the Paleogene source rocks in Bozhong Sag, Bohai Bay Basin. *Bull. Geol. Sci. Technol.* **2022**, *41*, 180–192. [CrossRef]
10. Schieber, J. Distribution and deposition of mudstone facies in the Upper Devonian Sonyea Group of New York. *J. Sediment. Res.* **1999**, *69*, 909–925. [CrossRef]
11. Hickey, J.J.; Henk, B. Lithofacies summary of the Mississippian Barnett Shale, Mitchell 2 TP Sims well, Wise County, Texas. *AAPG Bull.* **2007**, *91*, 437–443. [CrossRef]
12. Loucks, R.G.; Ruppel, S.C. Mississippian Barnett Shale: Lithofacies and depositional setting of a deep-water shale-gas succession in the Fort Worth Basin, Texas. *AAPG Bull.* **2007**, *91*, 579–601.
13. Niu, C.M.; Yu, H.B.; Hu, A.W.; Ye, T.; Qin, D.H.; Hua, X.L.; Liang, S.Y. Main controlling factors of natural gas accumulation and favorable exploration target in Bozhong Depression, Bohai Bay Basin. *China Pet. Explor.* **2021**, *26*, 152–164.
14. Yang, H.; Liu, C.L.; Wang, F.L.; Tang, G.M.; Li, G.X.; Zheng, X.X.; Wu, Y.P. Paleoenvironment and development model of source rocks of Dongying Formation in Bozhong Sag. *Lithol. Reserv.* **2021**, *33*, 81–92.
15. Song, Z.; Li, J.; Li, X.; Chen, K.; Wang, C.; Li, P.; Geng, H. Coupling Relationship between Lithofacies and Brittleness of the Shale Oil Reservoir: A Case Study of the Shahejie Formation in the Raoyang Sag. *Geofluids* **2022**, *2022*, 2729597. [CrossRef]
16. Han, G.; Cao, C.; Zhang, W.J.; Cao, Y.; Wang, S.H.; Bao, L. Hydrocarbon transport capacity of fault-sandstone configuration of Ed_{2+3} members in Liuchu area of Raoyang Sag and its relationship with oil and gas enrichment. *China Pet. Explor.* **2021**, *26*, 69–76.
17. Ji, Y.L.; Ren, H.Y.; Zhang, S.Q.; Ma, Z.T.; Niu, J.Y.; Guo, S.S.; Liu, X.Y. Paleogene palaeogeography and oil and gas distribution in Bohai Bay Basin. *J. Palaeogeogr. (Chin. Ed.)* **2022**, *24*, 611–633.
18. Lv, C.B.; Wu, Z.Y.; Liang, X.R.; Fu, L.L.; Pang, H.; Li, Q.; Lv, X.W. The Division of Reservoir Unit and Its Geological Significance in Lixian Slope of Raoyang Sag. *Sci. Technol. Eng.* **2020**, *20*, 6812–6821.
19. Song, J.; Huo, Z.; Fu, G.; Hu, M.; Liu, L. Petroleum migration and accumulation in the Liuchu area of Raoyang Sag, Bohai Bay Basin, China. *J. Pet. Sci. Eng.* **2020**, *192*, 107276.
20. Wei, Y.B.; Li, J.Q.; Lu, S.F.; Song, Z.J.; Zhao, R.X.; Zhang, Y.; Liu, X. Comprehensive evaluation method of sweet spot zone in lacustrine shale oil reservoir and its application: A case study of shale oil in lower 1st member of the Shahejie formation in the Raoyang sag. *J. China Univ. Min. Technol.* **2021**, *50*, 813–824. [CrossRef]
21. Tang, Y.J.; Zhang, H.F.; Ying, J.F.; Zhang, J.; Liu, X.M. Refertilization of ancient lithospheric mantle beneath the central North China Craton: Evidence from petrology and geochemistry of peridotite xenoliths. *Lithos* **2008**, *101*, 435–452.
22. Zhang, H.F.; Sun, M.; Zhou, X.H.; Zhou, M.F.; Fan, W.M.; Zheng, J.P. Secular evolution of the lithosphere beneath the eastern North China Craton: Evidence from Mesozoic basalts and high-Mg andesites. *Geochim. Cosmochim. Acta* **2003**, *67*, 4373–4387.
23. Chen, H.H.; Zhu, X.M.; Huang, H.D.; Shi, R.S.; Luo, Y.N.; Cui, G. Sediment Provenance of Shahejie Formation in Lixian Slope of Raoyang Depression Based on the Detrital Zircon Dating Analysis. *Earth Sci.* **2017**, *42*, 1955–1971.
24. Yang, F.; Wang, Q.; Hao, F.; Guo, L.X.; Zou, H.Y. Biomarker Characteristics of Lower Sub-Member of the First Member of the Shahejie Formation and Its Accumulation Contribution in Raoyang Depression, Jizhong Sub-Basin. *Lithol. Reserv.* **2021**, *46*, 172–185.

25. Zhang, C.H.; Han, J.Z.; Ji, Y.L.; Zhou, Y.; Su, B.; Wang, S.C.; Liu, J.X. Distribution characteristics and stacking patterns of sandbodies in the continental lacustrine fan delta-beach dam system: A case study from submember 3 upper of Paleogene Shahejie Formation in Liuxi area, Raoyang Sag, Bohai Bay Basin. *Nat. Gas Geosci.* **2020**, *31*, 518–531.
26. Du, W.; Ji, Y.L.; Ji, M.Y.; Jin, Z.G.; Hao, L.S.; Ran, A.H.; Yin, T.H. Establishment and significance of high-resolution Early Oligocene chronostratigraphic framework in Raoyang Sag, Bohai Bay. *J. China Univ. Pet. (Ed. Nat. Sci.)* **2020**, *44*, 142–151.
27. Wang, J.; Ma, S.P.; Luo, Q.; Guo, J.Y.; Cui, Z.Q. Recognition and resource potential of source rocks in Raoyang Sag of Bohai Bay Basin. *Acta Pet. Sin.* **2009**, *30*, 51–55.
28. Du, Y.F.; Zhu, X.M.; Ye, L.; Gao, Y. Features and Model of Mixed Sediments in Lower Submember of First Member of Shahejie Formation in Lixian Slope, Raoyang Sag. *Earth Sci.* **2020**, *45*, 3759–3778.
29. Xue, H.; Han, C.Y.; Xiao, B.Y.; Wang, F.; Li, L. Sedimentary characteristics and models of shallow water delta front of the lower first member of Shahejie Formation in Gaoyang area, Lixian Slope. *Lithol. Reserv.* **2020**, *32*, 69–80.
30. Geng, M.Y.; Chen, S.P.; Liu, L.F.; Huang, S.B.; Wu, B.; Zhang, Y. The palaeolake environment and development model of Paleogene high quality source rocks in the Bozhong Depression. *J. Northeast Pet. Univ.* **2021**, *45*, 10–21.
31. Du, Y.F.; Zhu, X.M.; Gao, Y.; Li, L.L.; Ye, L.; Li, X.D.; Chen, Y.Q. Sedimentary provenance of the first member of the Shahejie Formation, Lixian Slope, Raoyang Sag. *Earth Sci. Front.* **2021**, *28*, 115–130. [CrossRef]
32. Demaison, G.J.; Moore, G.T. Anoxic environments and oil source bed genesis. *AAPG Bull.* **1980**, *64*, 1179–1209.
33. Kelts, K. Environments of deposition of lacustrine petroleum source rocks: An introduction. *Geol. Soc. Lond. Spec. Publ.* **1988**, *40*, 3–26. [CrossRef]
34. Leng, M.J.; Marshall, J.D. Palaeoclimate interpretation of stable isotope data from lake sediment archives. *Quat. Sci. Rev.* **2004**, *23*, 811–831. [CrossRef]
35. Ma, Y.; Fan, M.; Lu, Y.; Liu, H.; Hao, Y.; Xie, Z. Climate-driven paleolimnological change controls lacustrine mudstone depositional process and organic matter accumulation: Constraints from lithofacies and geochemical studies in the Zhanhua Depression, eastern China. *Int. J. Coal Geol.* **2016**, *167*, 103–118.
36. Talbot, M.R. A review of the palaeohydrological interpretation of carbon and oxygen isotopic ratios in primary lacustrine carbonates. *Chem. Geol. Isot. Geosci. Sect.* **1990**, *80*, 261–279. [CrossRef]
37. Tribovillard, N.; Algeo, T.J.; Lyons, T.; Riboulleau, A. Trace metals as paleoredox and paleoproductivity proxies: An update. *Chem. Geol.* **2006**, *232*, 12–32. [CrossRef]
38. Yi, H.S.; Shi, Z.Q.; Zhu, Y.T.; Ma, X. Reconstruction of paleo-salinity and lake-level fluctuation history by using boron concentration in lacustrine mudstones. *J. Lake Sci.* **2009**, *21*, 77–83.
39. Ma, Y.; Fan, M.; Lu, Y.; Liu, H.; Hao, Y.; Xie, Z.; Hu, H. Middle Eocene paleohydrology of the Dongying Depression in eastern China from sedimentological and geochemical signatures of lacustrine mudstone. *Palaeogeogr. Palaeoclimatol. Palaeoecol.* **2017**, *479*, 16–33. [CrossRef]
40. Yan, M.C.; Chi, Q.H.; Gu, T.X.; Wang, C.S. Chemical Compositions of Continental Crust and Rocks in Eastern China. *Geophys. Geochem. Explor.* **1997**, *21*, 451–459.
41. Widayat, A.H.; Bas, V.; Oschmann, W.; Anggayana, K.; Püttmann, W. Climatic control on primary productivity changes during development of the Late Eocene Kiliran Jao Lake, Central Sumatra Basin, Indonesia. *Int. J. Coal Geol.* **2016**, *165*, 133–141.
42. Yin, J.; Wang, Q.; Hao, F.; Guo, L.X.; Zou, H.Y. Palaeoenvironmental reconstruction of lacustrine source rocks in the lower 1st Member of the Shahejie Formation in the Raoyang Sag and the Baxian Sag, Bohai Bay Basin, eastern China. *Palaeogeogr. Palaeoclimatol. Palaeoecol.* **2018**, *495*, 87–104. [CrossRef]
43. Yin, J.; Wang, Q.; Hao, F.; Guo, L.X.; Zou, H.Y. Palaeolake Environment and Depositional Model of Source Rocks of the Lower Submember of Sha1 in Raoyang Sag, Bohai Bay Basin. *Earth Sci.* **2017**, *42*, 1209–1222.
44. Schindler, D.W. Evolution of phosphorus limitation in lakes: Natural mechanisms compensate for deficiencies of nitrogen and carbon in eutrophied lakes. *Science* **1977**, *195*, 260–262.